

Niño 4 West (Niño-4W) Sea Surface Temperature Variability

Key Points:

- Niño-4W sea surface temperature (SST) variability, with high negative skewness, is a unique climate index in the western Pacific warm pool
- Zonal advective feedback, or advection due to anomalous zonal current, plays a key role in driving SST variability in Niño-4W
- Strong negative feedback from air-sea flux anomalies during the development of the warm events in Niño-4W contributes to the SST skewness

Supporting Information:

Supporting Information may be found in the online version of this article.

Correspondence to:


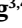



M. Feng,
Ming.Feng@csiro.au

Citation:

Feng, M., Zhang, Y., Hendon, H. H., McPhaden, M. J., & Marshall, A. G. (2021). Niño 4 west (Niño-4W) sea surface temperature variability. *Journal of Geophysical Research: Oceans*, 126, e2021JC017591. <https://doi.org/10.1029/2021JC017591>

Received 20 MAY 2021

Accepted 19 AUG 2021

Ming Feng^{1,2} , Ying Zhang^{3,4} , Harry H. Hendon⁵ , Michael J. McPhaden⁶ , and Andrew G. Marshall⁷ 

¹CSIRO Oceans and Atmosphere, Crawley, WA, Australia, ²Centre for Southern Hemisphere Oceans Research, Hobart, TAS, Australia, ³State Key Laboratory of Tropical Oceanography, South China Sea Institute of Oceanology, Chinese Academy of Sciences, Guangzhou, China, ⁴Southern Marine Science and Engineering Guangdong Laboratory, Guangzhou, China, ⁵Bureau of Meteorology, Melbourne, VIC, Australia, ⁶NOAA/Pacific Marine Environmental Laboratory, Seattle, WA, USA, ⁷Bureau of Meteorology, Hobart, TAS, Australia

Abstract Sea surface temperature (SST) variability in the western half of the Niño 4 region (Niño-4W), bounded by 160°E–175°W and 5°S–5°N, has a significant impact on weather and the marine environment of the Indo-Pacific. It exhibits significant negative skewness, with the strong penetration of the cold tongue into the western Pacific during strong La Niñas but a more muted response during El Niños. Zonal advection plays a dominant role in driving Niño-4W SST cooling during the strong La Niña events; vertical processes also contribute, with air-sea heat fluxes providing weak negative feedback. Advection also plays a key role in driving the Niño-4W SST warming, which is not always in sync with El Niño events. Among the advection terms, the advection of mean temperature by zonal velocity anomalies, or zonal advective feedback, plays a key role during the development phase of the warm and cold events. Strong negative air-sea heat flux anomalies during the development of warm events are linked to the negative SST skewness in the Niño-4W region.

Plain Language Summary Sea surface temperature variability in the western-central equatorial Pacific (the Niño-4W region) affects marine heatwaves and rainfall variability in Australia and other areas of the Indo-Pacific. In contrast with the central-eastern equatorial Pacific, negative temperature anomalies in the region tend to be stronger than positive temperature anomalies. This study used an upper ocean temperature budget analysis to reveal that zonal temperature advection plays a key role in driving surface temperature variability in the Niño-4W region. The high surface temperature in the warm pool may damp any further increase in ocean temperature in the region through air-sea heat flux adjustment.

1. Introduction

The weather and marine environments in the Indo-Pacific are highly sensitive to tropical Pacific climate variability, for example, El Niño Southern Oscillation (ENSO; McPhaden et al., 2006). We know though that ENSO events show great diversity. Traditional, or “eastern Pacific” (EP), El Niño events have strong eastern Pacific sea surface temperature (SST) warming, and Niño 3 region (150°W–90°W, 5°S–5°N) SST anomalies have been typically used to represent this type of El Niño (Yeh et al., 2009). In contrast, there is another variant with SST warming around the dateline in the central Pacific, the so-called “El Niño Modoki” or “central Pacific (CP) El Niño” (Ashok et al., 2007; Marathe et al., 2015), that is becoming more frequent in recent years (Freund et al., 2019; Yeh et al., 2009). These CP events play an important role in driving extreme climate conditions such as flooding and drought across the Asia-Pacific region (Cai et al., 2019; Di Lorenzo et al., 2010). The Niño 4 index, defined as the SST anomaly averaged within 160°E–150°W and 5°S–5°N, has been used to study the influences of the tropical Pacific climate variability on Australian rainfall (Feng & Li, 2011; Taschetto & England, 2009). Despite the generally dry conditions in Australia during El Niño events, Freund et al. (2021) showed that strong central Pacific El Niño events are also important for Australia’s Murray Darling Basin river catchment in leading to higher rainfall totals in southeastern Australia during the mature phase of El Niño, compared with weak central Pacific events, due to enhanced onshore flow from the Tasman Sea.

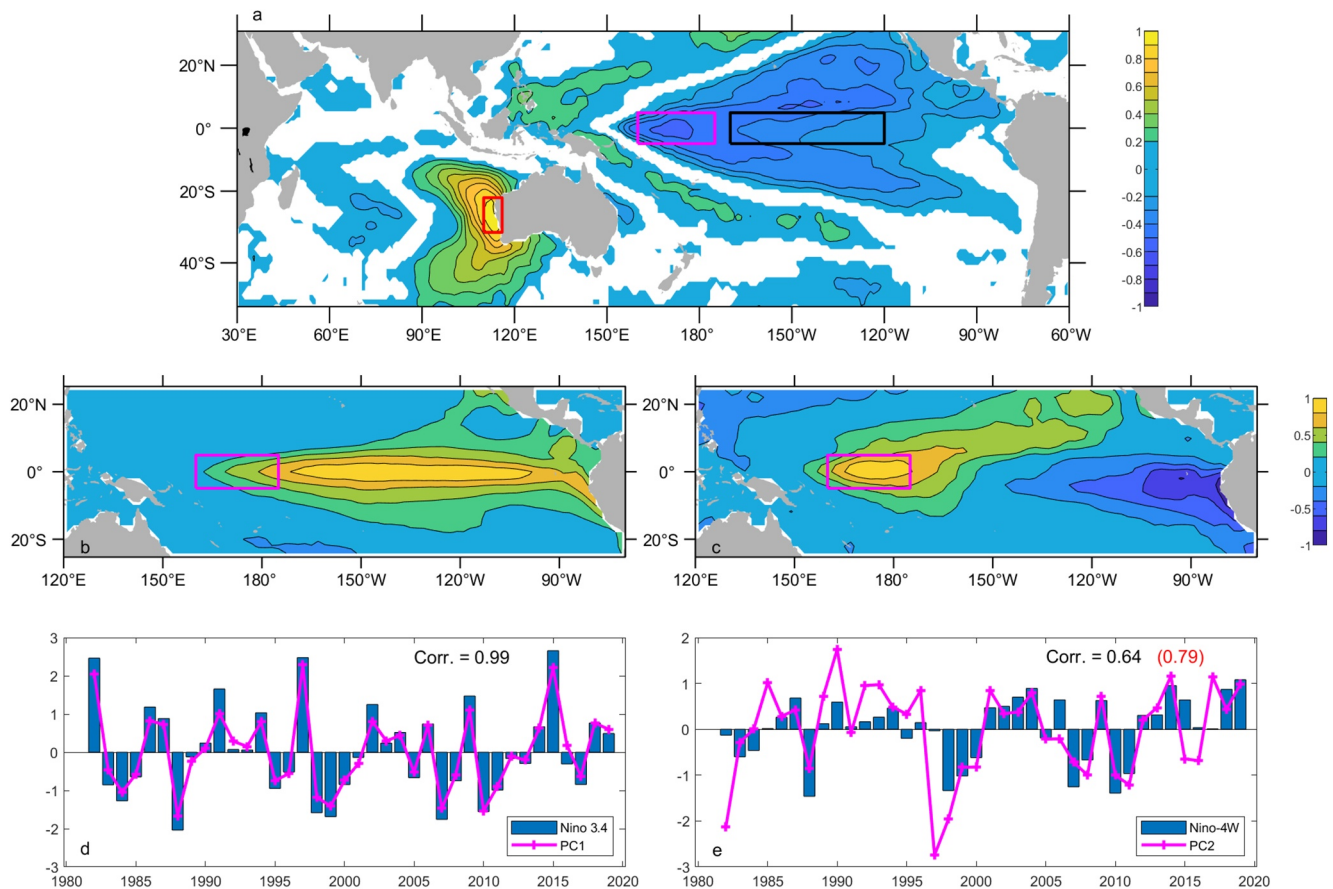


Figure 1. Pearson correlations (a) between the Ningaloo Niño index (32°S–22°S, 110°E–116°E average sea surface temperature [SST] anomalies) and SST anomalies in the Indo-Pacific Ocean during 1982–2020, and (b and c) top two empirical orthogonal function (EOF) modes of the tropical Pacific SST anomalies average during November–February, explaining 64% and 10% of the total variance, respectively. Panels (c) and (d) show the comparison between the top two principal components (PC) and Niño 3.4 and Niño-4W SST anomalies. The correlations between the PCs and the Niño 3.4 and Niño-4W SST anomalies are denoted (the number in the parenthesis is the correlation between the PC-2 and Niño-4W SST anomalies after 1998). The red, magenta, and black boxes in (a) denote the Ningaloo Niño, Niño-4W, and Niño 3.4 regions, respectively.

The eastern half of the Niño 4 region has been historically incorporated with the western half of the Niño 3 region into the so-called Niño 3.4 index to provide a unified representation of ENSO extremity. However, in recent years, SST variability in the western half of the Niño 4 region (which we refer to as Niño-4W, bounded by 160°E–175°W and 5°S–5°N) has been identified by Marshall et al. (2015) to be important in initiating Ningaloo Niño, marine heatwave events, via inducing cyclonic westerly anomalies over the southeast tropical Indian Ocean and instigating SST feedback, to strengthen the Leeuwin Current warm advection (Feng et al., 2013; Tozuka et al., 2021). The Niño-4W and associated wind anomalies are highly correlated with the Ningaloo Niño variability, on interannual to decadal time scales (Feng et al., 2021; Zhang & Han, 2018, Figure 1a). Using an atmospheric general circulation model (GCM) forced by SST anomalies associated with the Ningaloo Niño and the central Pacific, two-way interaction between the southeast Indian Ocean and the central equatorial Pacific, centered around the Niño-4W region (Zhang & Han, 2018), has been identified. This study confirmed the active role of Niño-4W SST in driving wind anomalies in the western equatorial Pacific and influencing the southeast Indian Ocean through both the Indonesian Throughflow and the atmospheric bridge. Zonal wind variability in the Niño-4W region is also the highest in the equatorial Pacific (Nagura & McPhaden, 2021).

The West Pacific SST gradient (WPG), defined as the standardized difference between area-averaged SST over the central Pacific Ocean (Niño-4 region) and west Pacific Ocean (0°–10°N, 130°–150°E), has been found to significantly modulate Indo-Pacific climate (Hoell & Funk, 2013) and Ningaloo Niño variability (Zinke et al., 2015). Moisture fluxes from the Niño-4W region, especially in austral winter-spring, may have a great influence on the northern Australian rainfall during austral summer (Rathore et al., 2020, 2021).

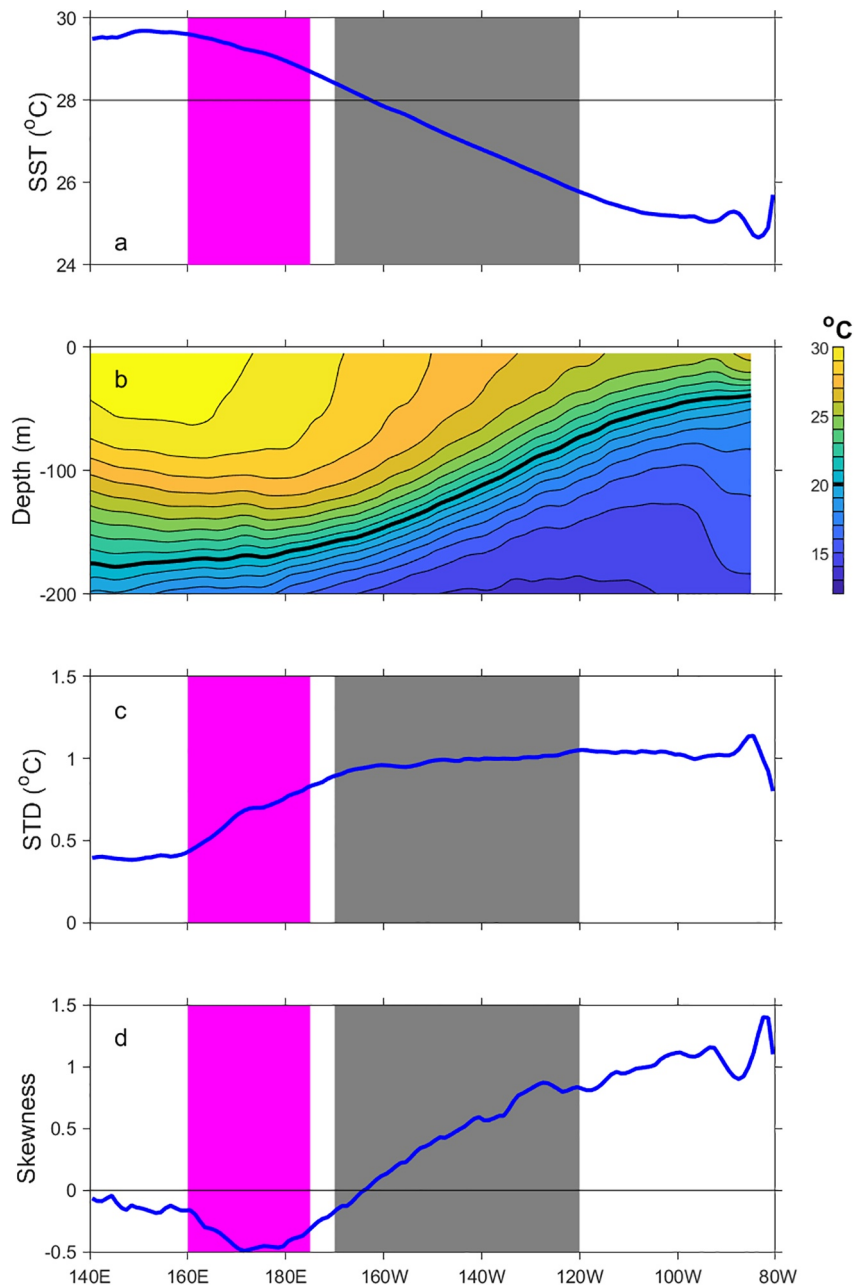


Figure 2. Mean (a) sea surface temperature (SST) and (b) upper ocean temperature, and (c) standard deviations and (d) skewness of SST anomalies along the equatorial Pacific during 1982–2020. SST is averaged within 5°N/S of the equator and monthly climatology during the same period is subtracted to obtain the anomaly field. Upper-ocean temperatures are averaged within 2°N/S of the equator. The heavy black line in (b) denotes the 20°C isotherm. The gray and magenta shadings denote the Niño 3.4 and Niño-4W regions, respectively.

An attempt to distinguish El Niño Modoki according to their influence on southern China rainfall also identified one type of El Niño Modoki with warming in the eastern half of Niño 4 versus a second type of asymmetric warming with a footprint in the western half of Niño 4 (Wang & Wang, 2013). An empirical orthogonal function (EOF) analysis of the November–February average SST anomalies suggests that while the first EOF represents the Niño 3.4 variability, the maximum loading of the second EOF is in the Niño-4W region (Figures 1b–1e), denoting its independence from the EP ENSO variability.

Since Niño-4W is being used with increasing frequency as a climate index, the purpose of this study is to provide a better understanding of SST variability and processes associated with the surface layer heat bal-

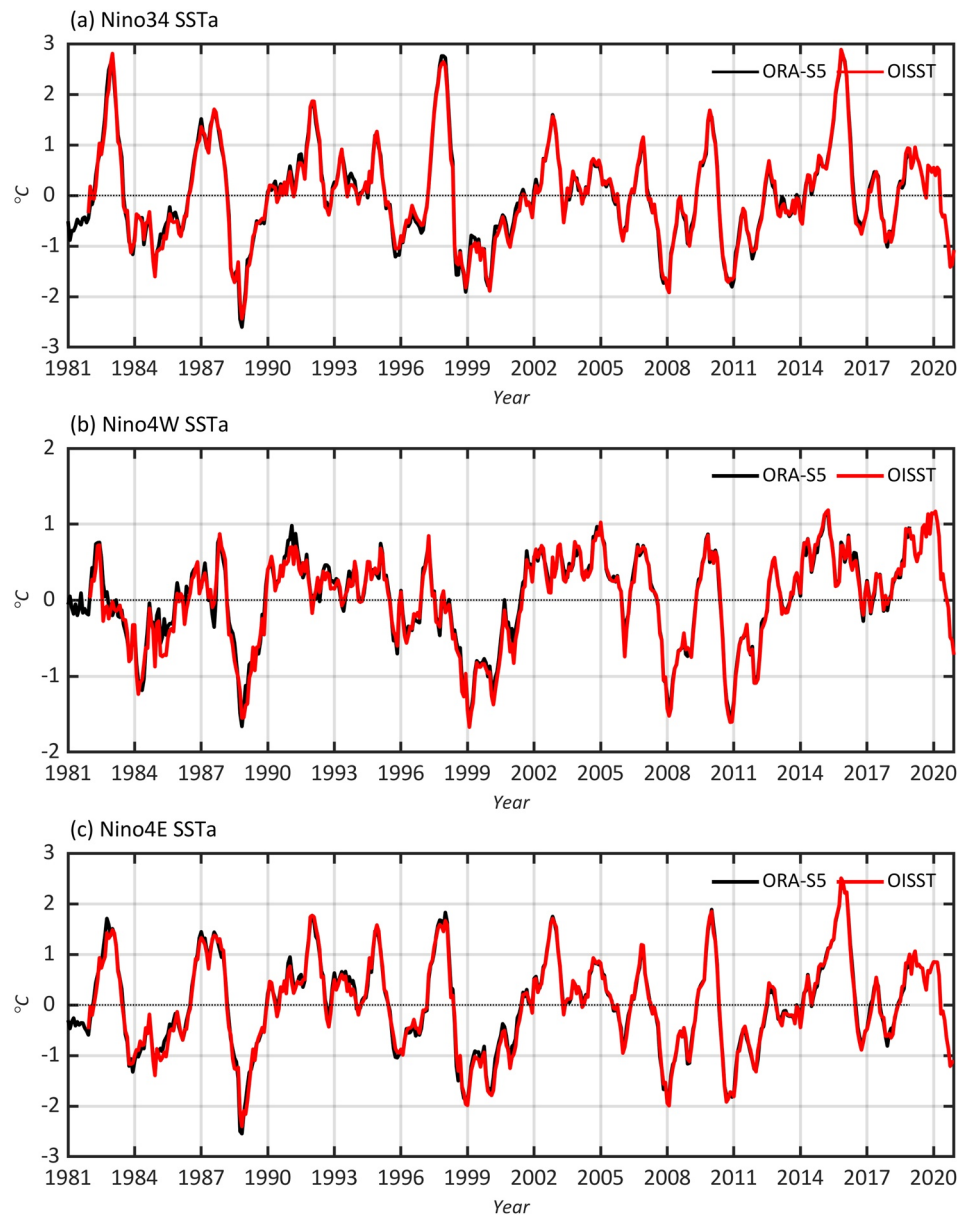


Figure 3. Comparison between ORA-S5 sea surface temperature (SST) and OISST anomalies in the (a) Niño 3.4, (b) Niño-4W, and (c) Niño-4E regions.

ance in this region. Thus, in this study, we will compare and contrast the statistics of SST variability in this region with other Niño regions. We will also examine the heat balance in the upper 50 m of the Niño-4W region to better understand the mechanisms responsible for SST variability there.

2. Data and Methods

We use the European Center for Medium-Range Weather Forecasts (ECMWF) OCEAN5 system, which is a new global eddy-permitting ocean-sea ice ensemble Ocean ReAnalysis System (ORA-S5, Zuo et al., 2019), to examine the Niño-4W heat balance. ORA-S5 uses an ocean model with eddy-permitting resolution (0.25°) in the horizontal and a near-surface resolution of 1 m in the vertical and covers the period from 1979–2018. The atmospheric reanalysis ERA-Interim (Dee et al., 2011) and ECMWF operational NWP are used as the forcing for ORA-S5 based on revised CORE bulk formulas (Large & Yeager, 2009) that include the impact of surface waves on the exchange of momentum and turbulent kinetic energy (Breivik et al., 2015). The

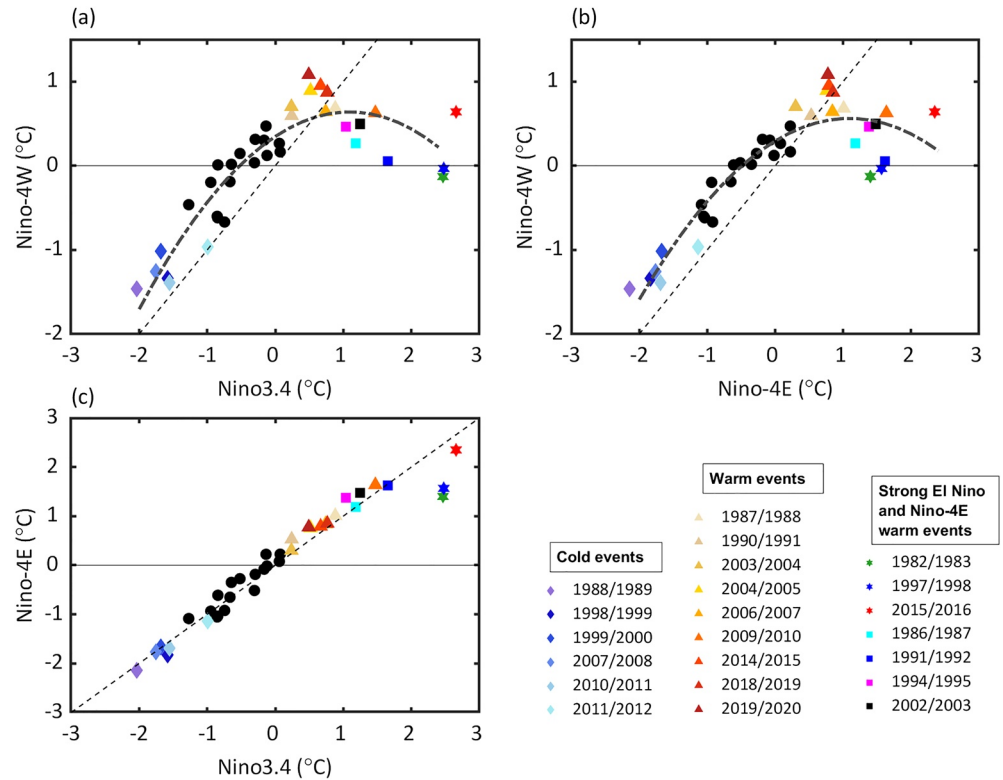


Figure 4. Scatter plots between November–February averaged (a) Niño 3.4 and Niño-4W, (b) Niño-4E and Niño-4W, and (c) Niño 3.4 and Niño-4E SST anomalies during 1982–2020, as derived from OISST. The dashed lines denote equal diagonals and the dashed-dotted curves in (a) and (b) are parabolic fits of the relationships. The colored years denote the warm and cold events in the Niño-4W region based on 0.6°C and −0.9°C criteria, and the three extreme El Niño and other warm events in Niño-4E.

observations including SST, sea-ice concentration, and in situ observations are simulated using a 5-day assimilation cycle, which consists of one outer iteration of 3D-Var FGAT with observation quality control and bias correction steps (Zuo et al., 2019).

The surface temperature budget is based on ORA-S5. Following Lee et al. (2004), we define \bar{T} as the average temperature in the upper 50 m within a control box at each month, and $\tilde{T} = T - \bar{T}$ as the deviation from the average in that month. After decomposing the velocity and temperature into mean seasonal climatology and eddy perturbations (e.g., $\tilde{T} = \tilde{T}_m + \tilde{T}'$), the perturbation temperature equation can be written as

$$\frac{\partial \tilde{T}'}{\partial t} = \frac{Q_{net}'}{\rho c_p H} + u_m \tilde{T}' + u' \tilde{T}_m + u' \tilde{T}' + v_m \tilde{T}' + v' \tilde{T}_m + v' \tilde{T}' + w_m \tilde{T}' + w' \tilde{T}_m + w' \tilde{T}' + Res.,$$

Table 1
Warm and Cold Events in the Niño 3.4, Niño-4E, and Niño-4W Regions, Indexed by the Year of Onset

Niño-4W warm years	1987, 1990, 2003, 2004, 2006, 2009 , 2014, 2015 , 2018, 2019
Niño-4E warm years	1982 , 1986, 1991 , 1994, 1997 , 2002, 2009 , 2015
Strong El Niño	1982 , 1991 , 1997 , 2009 , 2015
Niño-4W cold years	1988, 1998, 1999, 2007, 2010, 2011
Niño-4E cold years	1988, 1998, 1999, 2007, 2010, 2011
Strong La Niña	1988, 1998, 1999, 2007, 2010

Note. Niño-4W warm/cold events are selected for November–February average sea surface temperature (SST) anomalies greater/less than 0.6°C/−0.9°C. For Niño-4E, the criteria are 1.1°C/−1.1°C. Strong El Niño (in bold) and La Niña events are defined following Santoso et al. (2017).

Table 2
Linear Correlations Between the Niño-4W, Niño-4E, and Niño 3.4 Sea Surface Temperature (SST) Anomalies

	Niño-4W	Niño-4E	Niño 3.4
Niño-4W	1	0.79	0.67
Niño-4E		1	0.96
Niño 3.4			1

where the advection terms are calculated across the open boundaries of the control box (e.g., east, west, north, south, and bottom):

$$u_m \tilde{T}' = -\left(u'_{Em} \tilde{T}'_E - u'_{Wm} \tilde{T}'_W\right)$$

$$u' \tilde{T}'_m = -\left(u'_E \tilde{T}'_{Em} - u'_W \tilde{T}'_{Wm}\right)$$

$$u' \tilde{T}' = -\left(u'_E \tilde{T}'_E - u'_W \tilde{T}'_W\right)$$

Here, E and W are the east and west boundaries of the box, such as \tilde{T}_{Em} is the seasonal climatology of \tilde{T} at the east boundary and \tilde{T}'_E is the deviation from the climatology, and so on. Q_{net} is net air-sea heat flux subtracting the penetrating solar radiation at 50 m.

The meridional and vertical advection terms are decomposed similarly, which are grouped to represent the shallow overturning process. The residual mainly contains the turbulent mixing at the base of the layer and the horizontal mixing terms. Note that ORA-S5 does not completely conserve heat because of the way data are assimilated so some of the residuals in the heat balance may be due to the assimilation method. According to Lee et al. (2004), the total advection from this method is the same as the traditional method, however, it generally produces a better closure of the temperature budget. The method has been widely used in SST budget and feedback analysis in tropical oceans (e.g., Alory & Meyers, 2009; Guan & McPhaden, 2016).

Remotely sensed NOAA OISST data set v2.1 (Banzon et al., 2020; Reynolds et al., 2007), a global monthly SST data set with $1/4^\circ$ spatial resolution, and ORA-S5 SST are used to define SST indices in various boxes, the Niño-4W: $160^\circ E-175^\circ W$, $5^\circ S-5^\circ N$, Niño-4E (eastern half of the Niño 4 region): $175^\circ W-150^\circ W$, $5^\circ S-5^\circ N$, and Niño 3.4: $170^\circ W-120^\circ W$, $5^\circ S-5^\circ N$. EN4 is a reprocessed observational data set with globally quality-controlled ocean temperature/salinity profiles (Good et al., 2013). It includes all conventional oceanic observations (Argo, XBT, and MBT, conductivity-temperature-depth (CTD), moored buoys, and ship and mammal-based measurements). We use a gridded production from EN4 to examine correlations between surface and subsurface temperatures. Finally, we use the Climate Prediction Center Merged Analysis of Precipitation monthly data set (CMAP; Xie & Arkin, 1997) to assess relationships to global rainfall.

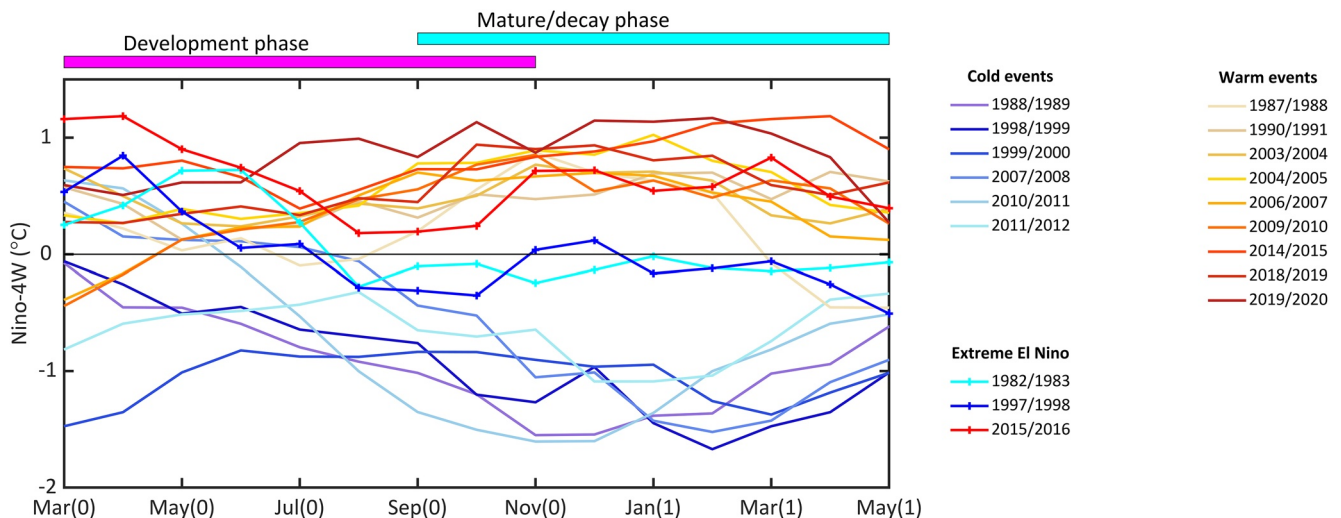


Figure 5. Sea surface temperature (SST) anomalies during the warm and cold events in the Niño-4W region, and the three extreme El Niños. The year of onset is labeled as year 0 and the decay year is labeled as year 1. The development phase for the budget study spans from March to November of year 0, and the mature/decay phase spans from September of year 0 to May in year 1.

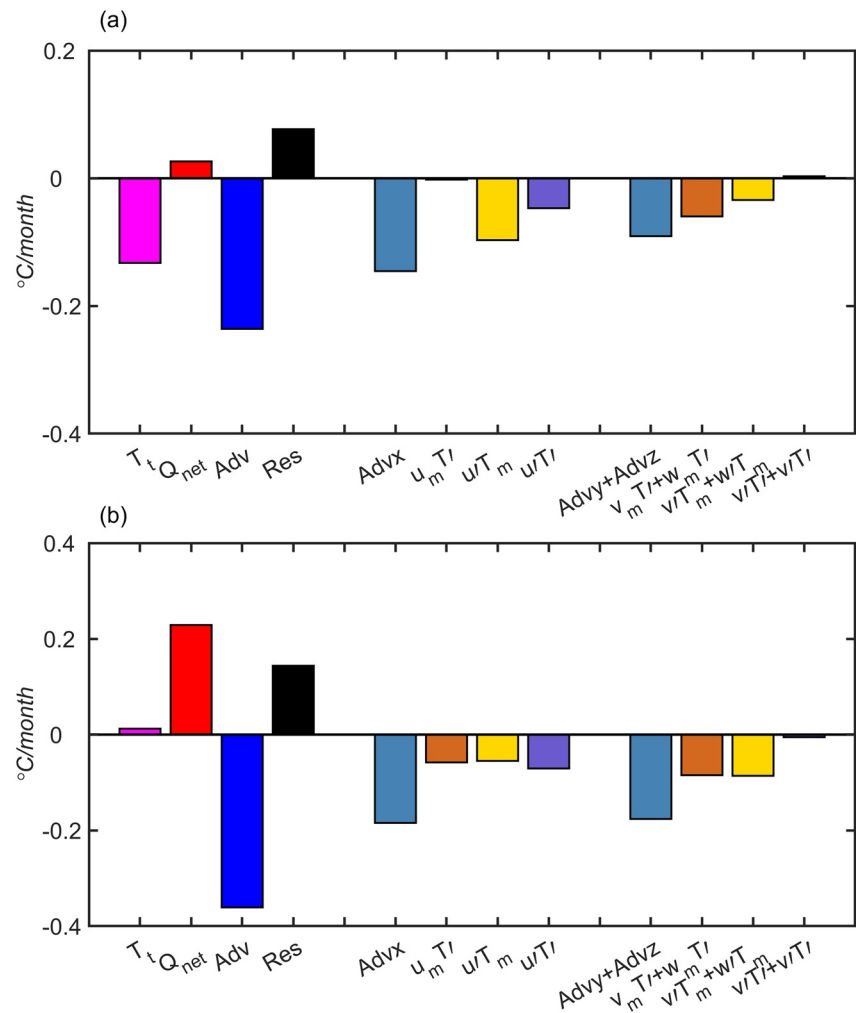


Figure 6. Upper 50 m temperature budget in the Niño-4W region during (a) the development (Mar–Nov [0]) and (b) mature/decay (Sep [0]–May [1]) phase of the cold events (six events including: 1988–1989, 1998–1999, 1999–2000, 2007–2008, 2010–2011, and 2011–2012).

3. Results

3.1. Characteristics of Interannual Variability

Along the equatorial Pacific, the prevailing easterly winds drive the equatorial upwelling in the east and pile up warm water in the west. The thermocline is deep in the western Pacific and shallow in the east, with the 20°C isotherm rises to shallower than 50 m in the eastern Pacific (Figure 2b). SST generally rises from east to west and west of 165°W, SST is on average above 28°C, the usual definition of the western Pacific warm pool (Figure 2a). The standard deviation of SST anomalies in the central-eastern equatorial Pacific is around 1°C, decreasing to less than 0.5°C in the far west (Figure 2c). It has been observed that SST anomalies have strong positive skewness in the eastern Pacific, due to extreme El Niño events (Figure 2d, Santoso et al., 2017). The skewness is defined as $m_3/m_2^{3/2}$, where m_3 and m_2 are the third and second moments of SST anomalies, following Burgers and Stephenson (1999).

The Niño-4W region is located within the western Pacific warm pool (with SST > 28°C), with a relatively weak zonal SST gradient compared with the Niño 3.4 region further east, and relatively deep and flat 20°C isotherm at ~180 m. Note that the shallower isotherms tilt slightly upward further west. The region has moderate SST variability in the equatorial Pacific and has the peak negative SST skewness, of up to –0.5 (Figure 2d). The negative SST skewness of the Niño 4 region has been noted in previous studies (Burgers &

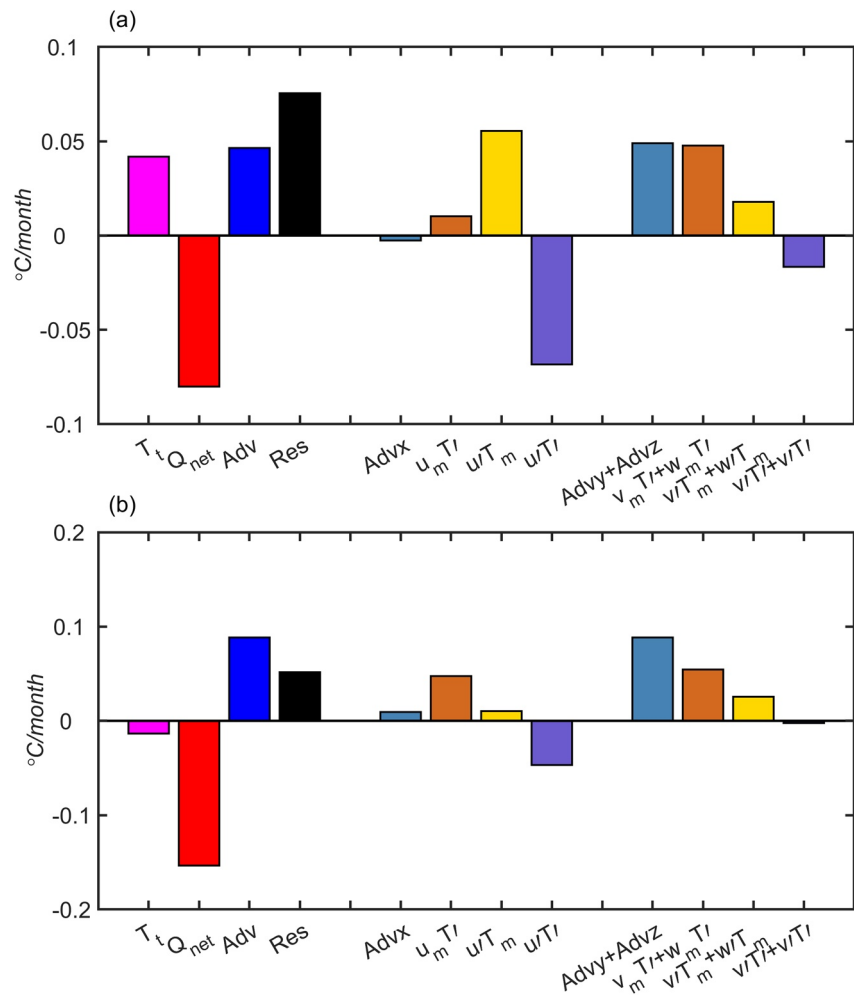


Figure 7. Upper 50 m temperature budget in the Niño-4W region during (a) the development and (b) mature/decay phases of the warm events (averaged over 1987–1988, 1990–1991, 2003–2004, 2004–2005, 2006–2007, 2009–2010, 2014–2015, 2015–2016 events).

Stephenson, 1999; Cai et al., 2019; Santoso et al., 2017), which has been attributed to the SST saturation in the warm pool (Burgers & Stephenson, 1999). However, the peak negative skewness mostly occurs in the Niño-4W region, the focus of this study.

The lagged correlation between the thermocline depth (D20) and SST anomalies is high in the eastern equatorial Pacific, >0.8 , denoting that the shallow thermocline can provide immediate feedback to the SST through vertical advection (Figure S1). There is an increased delay in the SST response to thermocline depth anomalies toward the dateline, due to planetary wave propagation as in previous analyses (e.g., Zelle et al., 2004). In the Niño-4W region, on the contrary, there is a negative correlation between the SST and thermocline depth, with the SST leading the temperature variability around 150 m by 2–12 months. This suggests that in the region, SST is unlikely to be strongly influenced by anomalous vertical advection.

SST variability from ORA-S5 is quite similar to that in OISST (Figure 3). Compared with Niño 3.4, where strong El Niño events tend to generate more significant positive SST anomalies (Figure 3a), the negative skewness of Niño-4W SST (-0.56) is due to the more significant negative SST anomalies during the strong La Niña events, comparing with the more muted warm events (Figure 3b). On the other hand, the Niño-4E SST is similar to Niño 3.4, but lacks positive skewness (0.45 for Niño 3.4 and zero for Niño-4E). Unlike Niño 3.4 and Niño-4E, where SST variability peaks in December–January,

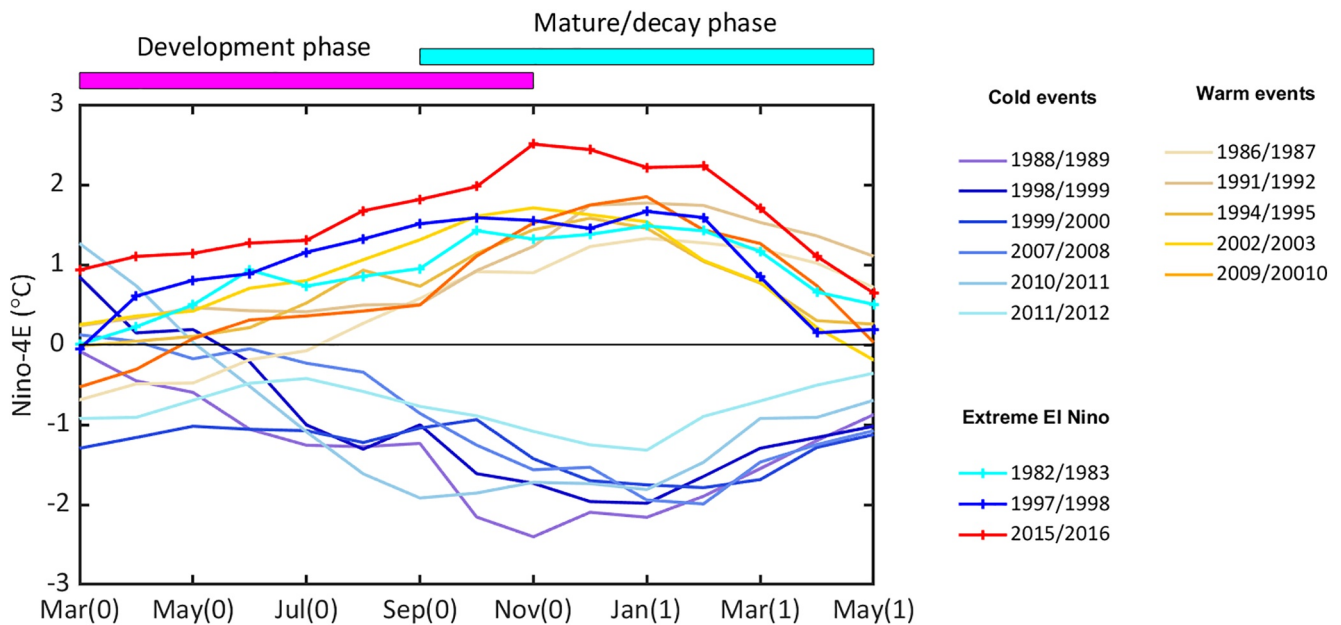


Figure 8. Sea surface temperature (SST) anomalies during the warm and cold events in the Niño-4E region, and the three extreme El Niños. The development year is labeled as year 0 and the decay year is labeled as year 1. The development phase for the budget study spans from March to November of year 0, and the mature/decay phase spans from September of year 0 to May in year 1.

Niño-4W SST variability has a weaker, but broader austral summer increase, with double peak values in November and February of more 0.7°C (Figure S2). On average, the standard deviation of the Niño-4W SST is about 0.6°C .

Niño-4W SST (averaged during November-February) appears to have a parabolic relationship compared to those either in Niño 3.4 or Niño-4E (Figures 4a and 4b). The relationship appears to be linear in the cold phase, with Niño-4W having weaker cold anomalies. Significant cold anomalies were generated in Niño-4W only during the strong La Niñas (strong negative Niño 3.4 SST; Table 1). The 2011–2012 moderate La Niña was also associated with a significant cold anomaly at Niño-4W, cooccurring with a strong Ningaloo Niño (Feng et al., 2015). On the other hand, the warm phases in Niño-4W are not in sync with either Niño 3.4 or Niño-4E. For example, no positive SST anomalies occurred in Niño-4W during the extreme 1982–1983 and 1997–1998 EP El Niños or the strong 1991–1992 El Niño. There was only a weak positive SST anomaly during the 2015–2016 extreme El Niño. 2009–2010 was the only other year that both Niño-4W and Niño-4E had significant warming, during a relatively strong central Pacific El Niño event (Figure 4, Table 1, Lee & McPhaden, 2010).

There appears to be a good linear relationship between the NDJF SST anomalies in Niño 3.4 and Niño-4E (Figure 4c), with the lack of positive skewness in Niño-4E most likely due to the weak SST anomalies during the 1982–1983 and 1997–1998 extreme El Niños. This is consistent with observations that SST signals associated with EP El Niño events do not extend westward into the warm pool region, except during CP El Niño or mixed type events (Santoso et al., 2017). Overall, the linear correlation between Niño-4W and Niño 3.4 indices was much lower than that between Niño-4E and Niño 3.4, which was close to 1 (Table 2).

All the warm events in Niño-4E are either EP or CP El Niños (Freund et al., 2021). On the other hand, several warm events in Niño-4W, for example, 1990–1991, 2003–2004, and 2018–2019, are not classified as El Niños. Most other Niño-4W events are CP El Niños, except the 2015–2016 event. Wang and Wang (2013) classified CP El Niño into two types based on the impacts on rainfall in China, which captured somewhat different events.

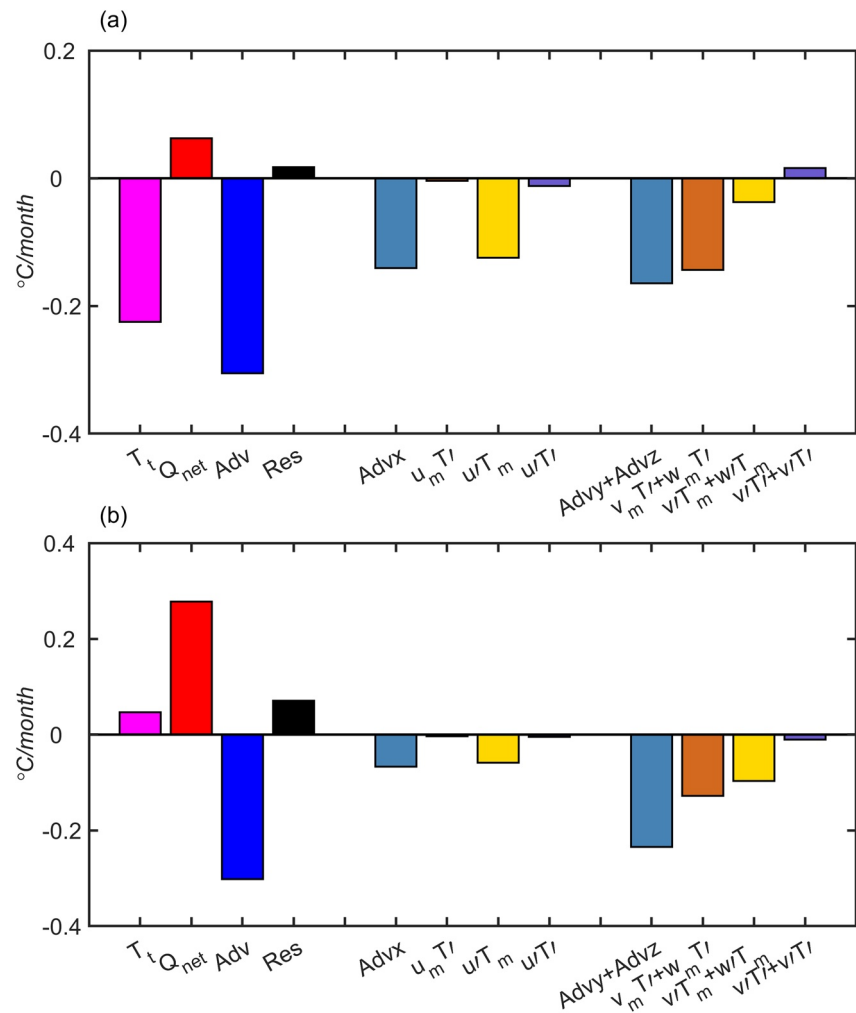


Figure 9. Upper 50 m temperature budget in the Niño-4E region during (a) the development (Mar–Nov [0]) and (b) mature/decay (Sep [0]–May [1]) phase of the cold events. Six events of which are included as in Table 1.

3.2. Heat Budget Analysis in the Niño-4W Region

3.2.1. Cold Events

The five strong La Niña events over the past several decades have negative SST anomalies of greater than 1°C in the Niño-4W region at a certain stage of their evolution, some peaking in November and some in February (Figure 5). SST anomalies in Niño-4W are small under all the other weak-moderate La Niña events, except the 2011–2012 event (Figure 3b). This is consistent with the observations that strong La Niña has a stronger western extension of the cold SST anomalies. The 1988–1989 and 2010–2011 events peaked in November, whereas the 1998–1999 and 2007–2008 events peaked in February. Note that the 1999–2000 La Niña evolved from a rather cold state in the Niño-4W region in early 1999, due to the nature of consecutive La Niña events during 1998–2000. The evolution of the 2011–2012 event might be influenced by the two-way interaction between the southeast Indian Ocean and Niño-4W, as proposed in Zhang and Han (2018).

During the development of Niño-4W cold events, which is defined as from March to November of year 0, anomalous surface temperature cooling in the Niño-4W region of 0.12°C per month during March–November is caused by the advection anomalies, with air-sea flux playing a minor compensating role (Figure 6a). The residual term, including turbulent mixing anomalies and numerical errors, also tend to counter the advective cooling. Note that if we exclude the 1999–2000 and 2011–2012 events, which start from a cold state, the composite temperature budget is largely balanced in the same way (Table S1). Both the anomalous

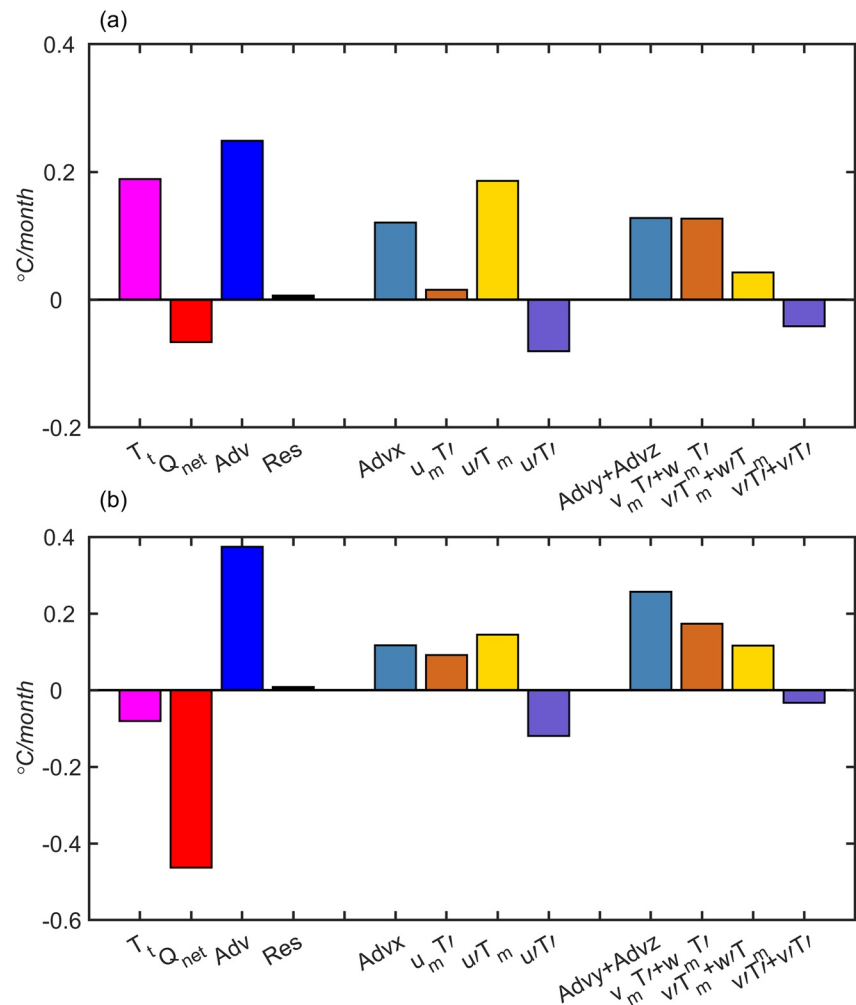


Figure 10. Upper 50 m temperature budget in the Niño-4E region during (a) the development (Mar–Nov [0]) and (b) mature/decay (Sep [0]–May [1]) phase of the warm events. Eight events of which are included as in Table 1.

advection and the surface temperature cooling are strongest during the development of the 2010–2011 event (Table S1), consistent with the unprecedented Ningaloo Niño event off the west coast of Australia (Feng et al., 2013).

During the mature/decay phase of the cold events, which is defined as from September of year 0 to May of year 1, anomalous advection continues to cool the Niño-4W region. It is balanced by air-sea flux anomaly and the residual, resulting in a weak warming tendency (Figure 6b, Table S2). Also, tropical instability waves are stronger and extend further west during La Niña events (e.g., Zheng et al., 2016; Wang et al., 2019), due to the strengthening of the South Equatorial Current (Johnson et al., 2002), which likely plays a role as negative feedback to cooling in the Niño-4W region.

Among the advection terms, zonal advection contributes the most during both the development and mature/decay phases of cold events (Figure 6). When decomposing the advection terms into velocity and temperature perturbations, anomalous zonal velocity acting on the mean temperature gradient, or the zonal advective feedback, is the main driver of SST cooling during the development phase (Figure 6). Nonlinear zonal advection also plays a secondary role. During the mature/decay phase, however, almost all the advection terms are important.

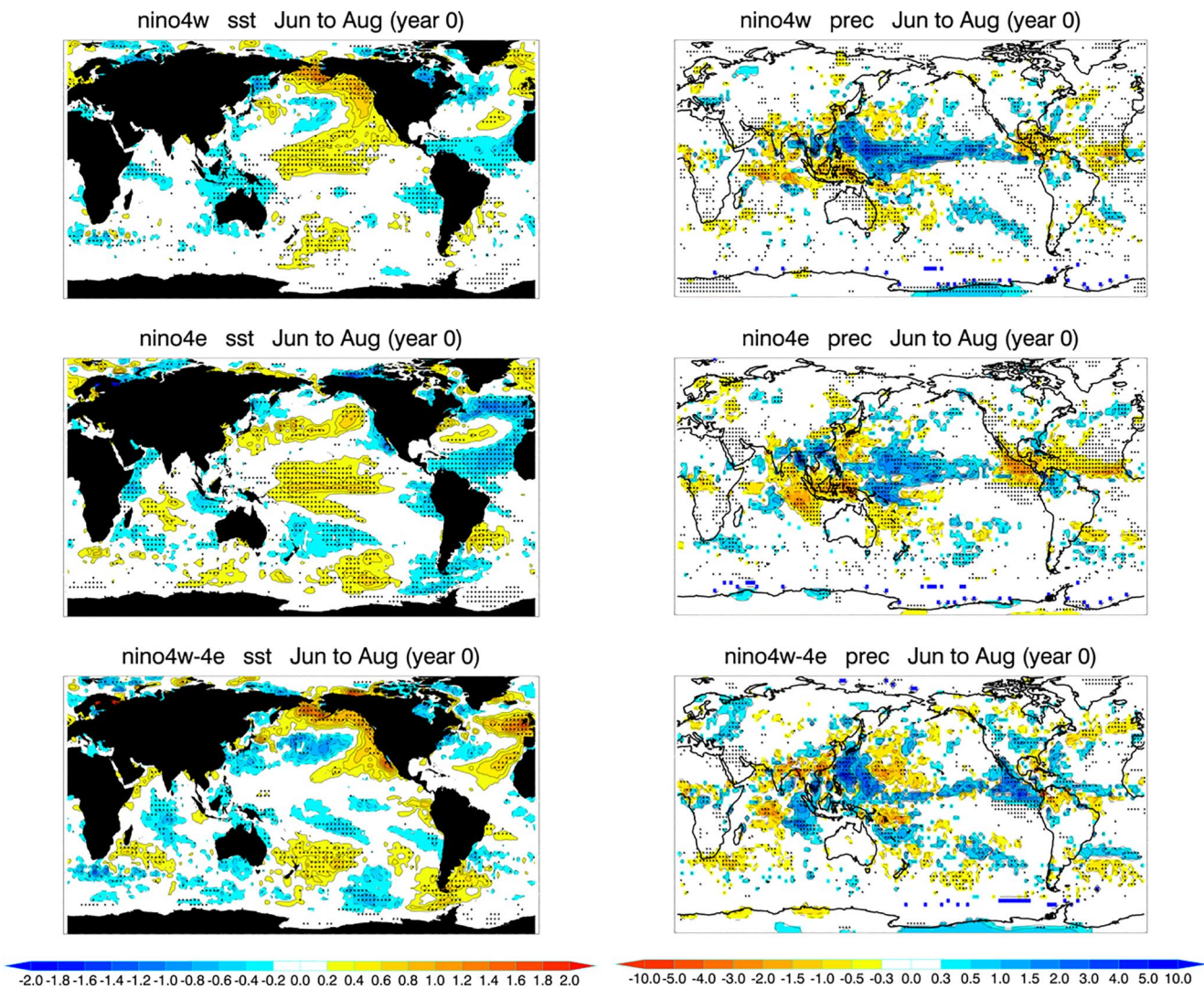


Figure 11. Sea surface temperature (SST) (left column) and precipitation (right column) anomaly composites for Niño-4W warm years (top row), Niño-4E warm years (middle row), and the Niño-4W minus Niño-4E difference (bottom row), during the June–August developing phase (year 0). Stippling indicates significantly different anomalies at 90% confidence levels using Student's (1908) *t*-test.

3.2.2. Warm Events

There were 10 warm events in the Niño-4W region over the observation period, noting that we use a NDJF SST anomaly criterion of 0.6°C (Figure 5). Limited by the availability of ORA-S5 model data, two recent warming events (2018–2019 and 2019–2020) are not considered in the budget analysis.

During the development phase of warm events, anomalous advection and the residual play the dominant role in warming the surface layer, whereas air-sea exchange acts as strong negative feedback to the warming (Figure 7). Among the advection terms, the zonal advective feedback and vertical advection associated with anomalous thermocline temperature, or thermocline feedback (Santoso et al., 2017), play dominant roles to warm the upper ocean, whereas nonlinear advective terms act to cool. During the mature/decay phase of warm events, anomalous air-sea flux tends to cool the surface ocean, which is mainly balance by the advection terms.

Compared to cold events, air-sea heat fluxes are substantially stronger negative feedback on the SST anomalies. Thus, it is likely that warm SSTs in the Niño-4W region limit further warming in the region, leading to the negative skewness of the SST anomalies there.

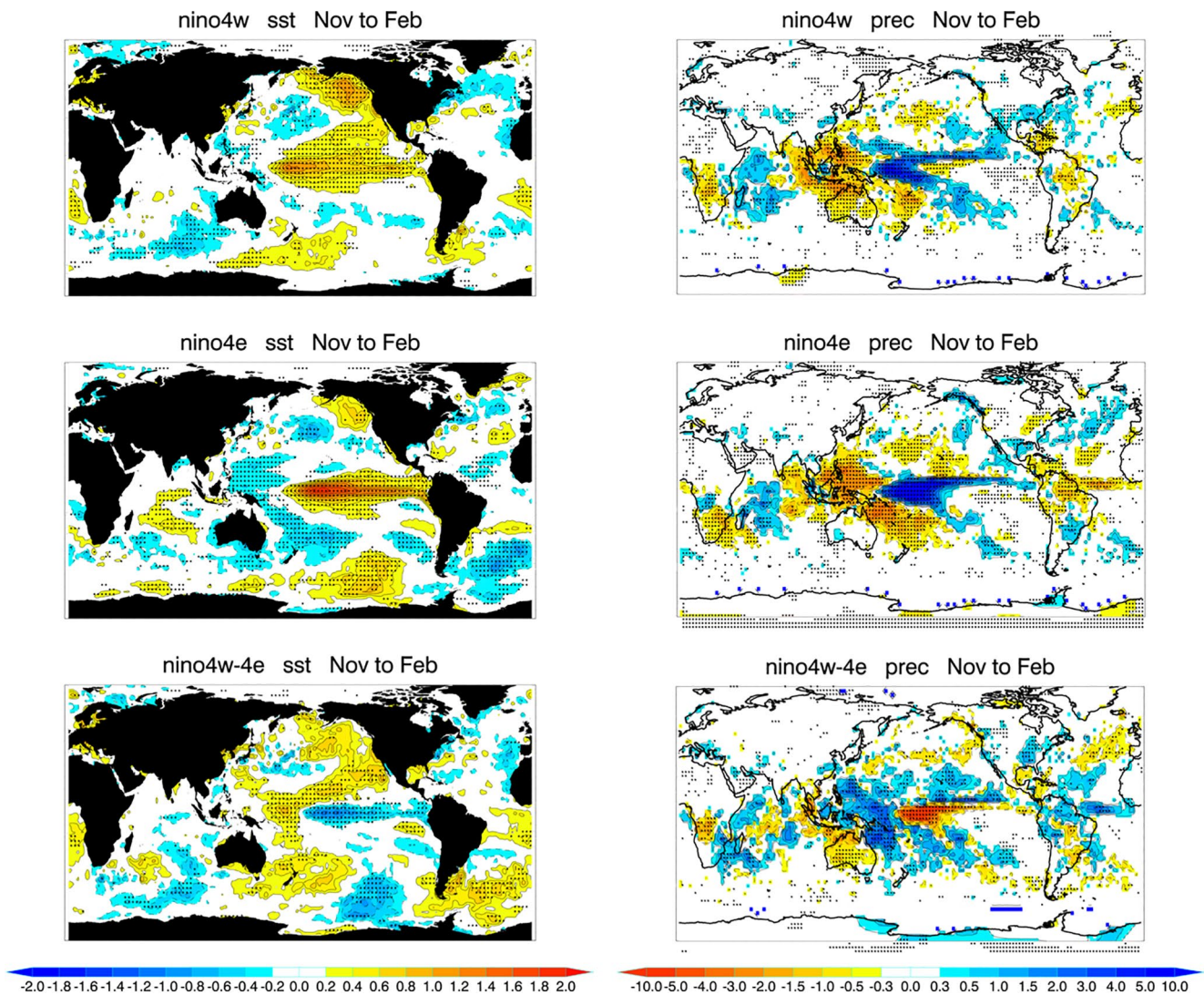


Figure 12. Same as Figure 11 but during the November–February peak phase.

3.3. Comparing With Niño-4E and Niño 3.4 SST Variability

Niño-4E cold events are the same as in Niño-4W, with the peak cold anomalies of about -2°C , except the 2011–202012 event, when the peak SST anomalies of just above -1°C occurred in January 2012 (Figure 8). All the extreme El Niño events caused $>1^{\circ}\text{C}$ warming, with the 2015–202016 event being the warmest during the austral summer period (Figure 8). Note that we use a higher threshold to define warm events in Niño-4E due to the higher SST standard deviation compared with Niño-4W.

The cooling tendency in Niño-4E during cold events is stronger than Niño-4W. Similar to Niño-4W, advection is still the key driver for the cooling in Niño-4E; however, the thermocline feedback becomes the dominant cooling term during both the development and mature/decay phases (Figure 9). For warm events, advection anomalies still drive the warming tendency, with the zonal advective feedback now playing a more dominant role (Figure 10). Air-sea fluxes still play a key role to counter the advection tendencies for both warm and cold events.

For completeness, we also carried out the SST budget calculation for the Niño 3.4 region for all the five strong El Niño events and five strong La Niña events, following Santoso et al. (2017). For both warm and cold events, SST tends to peak during the November–January period, with a peak amplitude of 2°C or higher

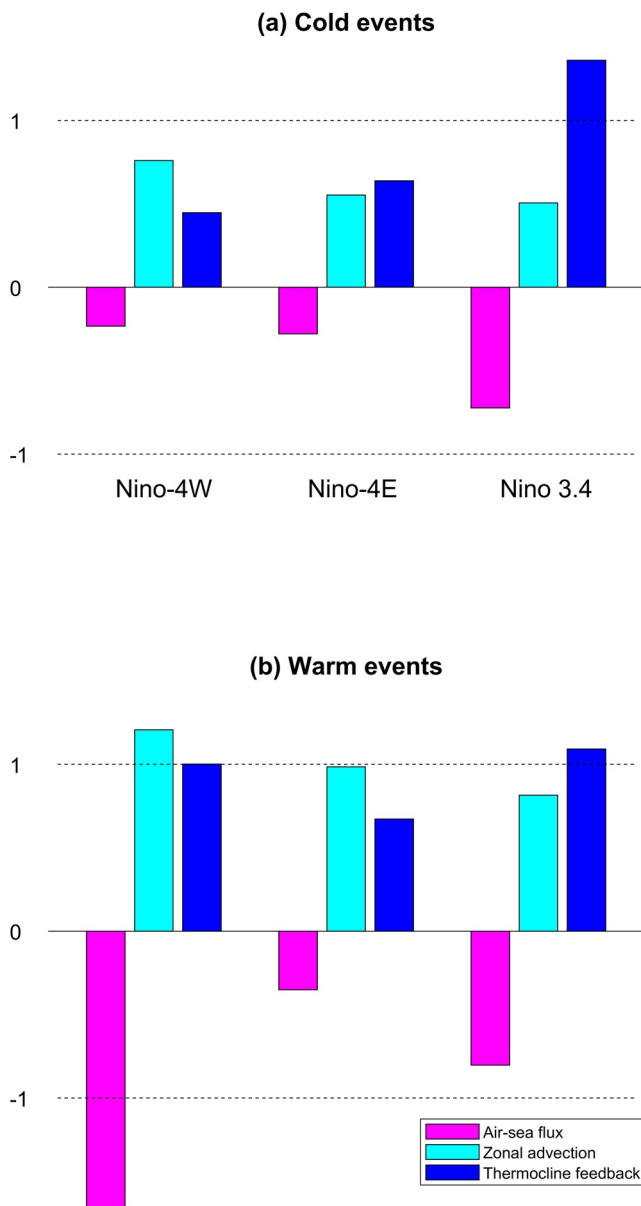


Figure 13. Ratios between the air-sea heat flux, zonal advection, and thermocline feedback anomalies and the temperature tendency term during the development phase of (a) cold and (b) warm events in the Niño-4W, Niño-4E, and Niño 3.4 regions.

during the extreme El Niños (Figure S3). For the Niño 3.4 region, the SST variations during both the development and mature/decay phases of the strong La Niña events are mostly driven by thermocline feedback, with the anomalous zonal advection also contributing to some extent during the development phase of the warm events (Figure S4). For El Niños, the thermocline feedback plays the most dominant role to drive the Niño 3.4 warming; however, zonal advective feedback plays an important secondary role during the development phase (Figure S5). The SST budget results remain the same when we shift the western boundary of the Niño-4W box eastward (Figures S6 and S7).

4. Summary and Discussion

In this study, we examined SST variability and the upper 50 m heat budget of a new climate index, the Niño-4W SST. SST anomalies in Niño-4W, the western half of the Niño 4 region, are important in generating wind anomalies in the southeast Indian Ocean through a two-way interaction, affecting the Ningaloo Niño evolution and regional climate in Australia and the Indonesian Seas. The region has moderate SST anomalies, with however the highest negative skewness in the equatorial Pacific, in contrast with the positive skewness in the eastern Pacific.

Warm events in Niño-4W were not in sync with those in Niño-4E or Niño 3.4, except for the strong 2009–2010 CP El Niño and the 2015–2016 extreme El Niño. On the other hand, only strong La Niñas can generate significant cooling anomalies in Niño-4W, mostly through the zonal advective feedback. This is also in contrast with the eastern Pacific where the thermocline feedback plays the dominant role in generating SST anomalies.

Furthermore, SST and rainfall teleconnections for Niño-4W warm events are distinct from those of Niño-4E warm events over many parts of the globe. Niño-4W warm years show higher rainfall in the western Pacific Ocean during both the development phase in boreal summer (Figure 11) and the peak phase in austral summer (Figure 12), compared to Niño-4E warm years. This is particularly prevalent in austral summer, consistent with the westward shifted peak in warm equatorial Pacific SST. Rainfall differences are also seen over continental landmasses, including over southern China in boreal summer (e.g., Wang & Wang, 2013, Figure S8), and notably over Australia in austral summer when Niño-4W warm events lead to anomalous drying over much of the continent (compared to average rainfall during Niño-4E warm years). The Australian summer signal appears to be associated not only with the teleconnection pathway from the central Pacific, but also with an upstream wave train teleconnection from the eastern Indian Ocean (not shown) where the SSTs are

cooler during Niño-4W warm years (Figure 12). This further points to the contemporaneous interaction between the southeast Indian Ocean and the central equatorial Pacific, centered around the Niño-4W region (Zhang & Han, 2018).

Relative to the temperature tendencies during the development phase of cold events, the thermocline feedback becomes relatively more important toward the east, whereas the zonal advection becomes less important in causing the negative SST anomalies to the east (Figure 13). The contrast is less striking for the development of the warm events among the three regions. Still, the zonal advection becomes less significant to the east. While the negative feedbacks from air-sea heat flux anomalies are on par between the cold and warm events in the Niño-4E and Niño 3.4 regions, the most significant negative feedback from the air-sea

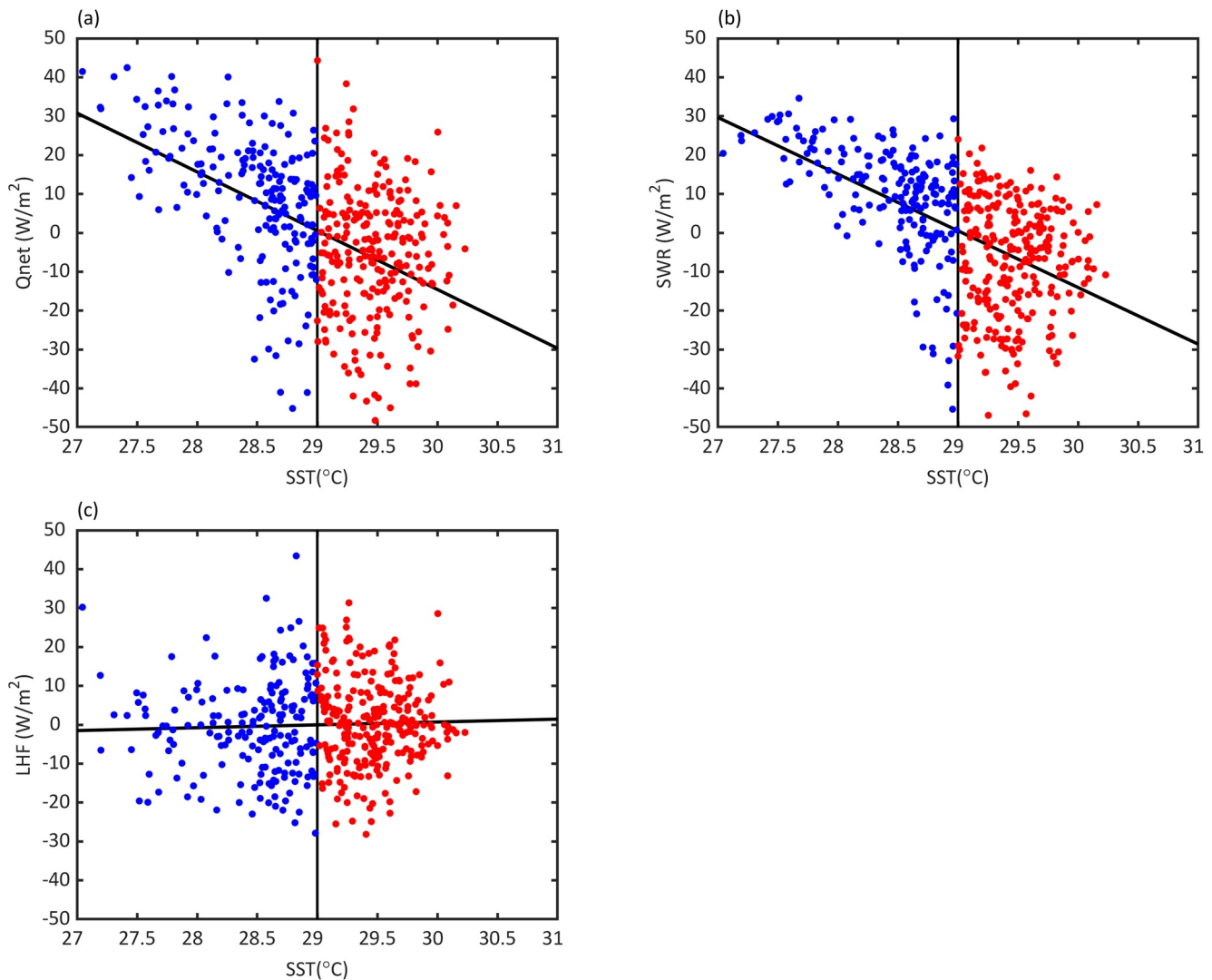


Figure 14. Scatter diagrams between (a) net heat flux, (b) shortwave radiation, (c) latent heat flux anomalies in Niño-4W against sea surface temperature (SST) in Niño-4W. Black lines denote the linear regression of net heat flux/shortwave radiation/latent heat flux anomalies against SST. Blue (red) dots are when SST is less (greater) than 29°C.

flux on warm events occurs in the Niño-4W region (Figure 13). The differences in the negative contributions from the air-sea heat flux between the warm and cold events in the Niño-4W region may contribute substantially to the negative skewness of the SST anomalies, consistent with early speculation that SST saturation may be the driver for negative skewness. We also note that the positive skewness in the Niño 3.4 region is likely due to the lack of matching negative air-sea flux anomalies during warm events to counterbalance strong thermocline feedbacks. The importance of the zonal advective feedback in CP Niño events and the importance of thermocline feedback in EP El Niño events is consistent with previous studies (Kug et al., 2009; Marathe et al., 2015). The budget analysis should be repeated with other reanalysis products due to uncertainties of different flux products which are used to drive the models (e.g., Marathe et al., 2015) and the sensitivity of the results to the choice of reanalysis product (e.g., Lübbecke & McPhaden, 2014).

It appears that the negative correlation between net heat flux anomalies and SST in the Niño-4W region was mostly due to shortwave variability (Figure 14), that is, large negative net heat flux anomalies under warm SST are also mostly due to the reduction in shortwave radiation. This is consistent with the negative feedback of air-sea heat fluxes on SST variability in Niño-4W, which is associated with the relationship between deep convection and SST in the warm pool region (e.g., Waliser & Graham, 1993) affecting the cloud

cover in the region. The asymmetric response of air-sea flux to SST warming and cooling in the Niño-4W may also involve regional air-sea coupling processes. The Clausius-Clapeyron effect on moisture and latent heat fluxes across the air-sea interface (e.g., Held & Soden, 2000; Liu, 1998) may play a role. Other factors may also contribute to the negative skewness in Niño-4W SST. The Niño-4W region has high surface salinity variance (Zhao et al., 2016), so that barrier layers due to salinity stratification in the surface mixed layer may contribute to the SST saturation in the region. The zonal migration of the low surface salinity pool may also have some effect. Note also that the high salinity variability may be associated with high wind variability in the region (Nagura & McPhaden, 2021) and associated evaporation variability that contributes to the moisture source of rainfall in the northern Australian region (Rathore et al., 2020).

Data Availability Statement

PMEL contribution no. 5262. ORA-S5 model outputs are available from <https://www.cen.uni-hamburg.de/icdc/data/ocean/easy-init-ocean/ecmwf-oras5.html>.

Acknowledgments

M. Feng was supported by the Center for Southern Hemisphere Oceans Research (CSHOR), which is a joint initiative between the Qingdao National Laboratory for Marine Science and Technology (QNLMT), CSIRO, University of New South Wales, and University of Tasmania. Ying ZHANG was supported by the Chinese Academy of Sciences (XDB42010305 and LTO-ZZ2005). We thank two anonymous reviewers for constructive comments.

References

- Alory, G., & Meyers, G. (2009). Warming of the upper equatorial Indian Ocean and changes in the heat budget (1960–99). *Journal of Climate*, 22(1), 93–113. <https://doi.org/10.1175/2008jcli2330.1>
- Ashok, K., Behera, S. K., Rao, S. A., Weng, H., & Yamagata, T. (2007). El Niño Modoki and its possible teleconnection. *Journal of Geophysical Research*, 112, C11007. <https://doi.org/10.1029/2006jc003798>
- Banzon, V., Smith, T. M., Steele, M., Huang, B., & Zhang, H.-M. (2020). Improved estimation of proxy sea surface temperature in the Arctic. *Journal of Atmospheric and Oceanic Technology*, 37, 341–349. <https://doi.org/10.1175/JTECH-D-19-0177.1>
- Breivik, Ø., Mogensén, K., Bidlot, J.-R., Balmaseda, M. A., & Janssen, P. A. (2015). Surface wave effects in the NEMO ocean model: Forced and coupled experiments. *Journal of Geophysical Research: Oceans*, 120, 2973–2992. <https://doi.org/10.1002/2014JC010565>
- Burgers, G., & Stephenson, D. B. (1999). The “normality” of El Niño. *Geophysical Research Letters*, 26(8), 1027–1030. <https://doi.org/10.1029/1999gl900161>
- Cai, W., Wu, L., Lengaigne, M., Li, T., McGregor, S., Kug, J. S., et al. (2019). Pantropical climate interactions. *Science*, 363(6430). <https://doi.org/10.1126/science.aav4236>
- Dee, D. P., Uppala, S. M., Simmons, A. J., Berrisford, P., Poli, P., Kobayashi, S., et al. (2011). The ERA-Interim reanalysis: Configuration and performance of the data assimilation system. *The Quarterly Journal of the Royal Meteorological Society*, 137, 553–597. <https://doi.org/10.1002/qj.828>
- Di Lorenzo, E., Cobb, K. M., Furtado, J. C., Schneider, N., Anderson, B. T., Bracco, A., et al. (2010). Central Pacific El Niño and decadal climate change in the North Pacific ocean. *Nature Geoscience*, 3(11), 762–765. <https://doi.org/10.1038/ngeo984>
- Feng, J., & Li, J. (2011). Influence of El Niño Modoki on spring rainfall over south China. *Journal of Geophysical Research*, 116(D13). <https://doi.org/10.1029/2010jd015160>
- Feng, M., Caputi, N., Chandrapavan, A., Chen, M., Hart, A., & Kangas, M. (2021). Multi-year marine cold-spells off the west coast of Australia and effects on fisheries. *Journal of Marine Systems*, 214, 103473. <https://doi.org/10.1016/j.jmarsys.2020.103473>
- Feng, M., Hendon, H. H., Xie, S. P., Marshall, A. G., Schiller, A., Kosaka, Y., et al. (2015). Decadal increase in Ningaloo Niño since the late 1990s. *Geophysical Research Letters*, 42(1), 104–112. <https://doi.org/10.1002/2014gl062509>
- Feng, M., McPhaden, M. J., Xie, S. P., & Hafner, J. (2013). La Niña forces unprecedented Leeuwin Current warming in 2011. *Scientific Reports*, 3(1), 1–9. <https://doi.org/10.1038/srep01277>
- Freund, M. B., Henley, B. J., Karoly, D. J., McGregor, H. V., Abram, N. J., & Dommenget, D. (2019). Higher frequency of Central Pacific El Niño events in recent decades relative to past centuries. *Nature Geoscience*, 12, 450–455. <https://doi.org/10.1038/s41561-019-0353-3>
- Freund, M. B., Marshall, A. G., Wheeler, M. C., & Brown, J. N. (2021). Central Pacific El Niño as a precursor to summer drought-breaking rainfall over southeastern Australia. *Geophysical Research Letters*, 48(7), e2020GL091131. <https://doi.org/10.1029/2020gl091131>
- Good, S. A., Martin, M. J., & Rayner, N. A. (2013). EN4: Quality controlled ocean temperature and salinity profiles and monthly objective analyses with uncertainty estimates. *Journal of Geophysical Research*, 118, 6704–6716. <https://doi.org/10.1002/2013JC009067>
- Guan, C., & McPhaden, M. J. (2016). Ocean processes affecting the twenty-first-century shift in ENSO SST variability. *Journal of Climate*, 29(19), 6861–6879. <https://doi.org/10.1175/jcli-d-15-0870.1>
- Held, I. M., & Soden, B. J. (2000). Water vapor feedback and global warming. *Annual Review of Energy and the Environment*, 25(1), 441–475. <https://doi.org/10.1146/annurev.energy.25.1.441>
- Hoell, A., & Funk, C. (2013). The ENSO-related west Pacific sea surface temperature gradient. *Journal of Climate*, 26(23), 9545–9562. <https://doi.org/10.1175/jcli-d-12-00344.1>
- Johnson, G. C., Sloyan, B. M., Kessler, W. S., & McTaggart, K. E. (2002). Direct measurements of upper ocean currents and water properties across the tropical Pacific during the 1990s. *Progress in Oceanography*, 52, 31–61. [https://doi.org/10.1016/s0079-6611\(02\)00021-6](https://doi.org/10.1016/s0079-6611(02)00021-6)
- Kug, J. S., Jin, F. F., & An, S. I. (2009). Two types of El Niño events: Cold tongue El Niño and warm pool El Niño. *Journal of Climate*, 22(6), 1499–1515. <https://doi.org/10.1175/2008jcli2624.1>
- Large, W. G., & Yeager, S. G. (2009). The global climatology of an interannually varying air–sea flux data set. *Climate Dynamics*, 33, 341–364. <https://doi.org/10.1007/s00382-008-0441-3>
- Lee, T., Fukumori, I., & Tang, B. (2004). Temperature advection: Internal versus external processes. *Journal of Physical Oceanography*, 34(8), 1936–1944. [https://doi.org/10.1175/1520-0485\(2004\)034<1936:taivep>2.0.co;2](https://doi.org/10.1175/1520-0485(2004)034<1936:taivep>2.0.co;2)

- Lee, T., & McPhaden, M. J. (2010). Increasing intensity of El Niño in the central-equatorial Pacific. *Geophysical Research Letters*, 37, L14603. <https://doi.org/10.1029/2010GL044007>
- Liu, W. T. (1988). Moisture and latent heat flux variabilities in the tropical Pacific derived from satellite data. *Journal of Geophysical Research: Oceans*, 93(C6), 6749–6760. <https://doi.org/10.1029/jc093ic06p06749>
- Lübbecke, J. F., & McPhaden, M. J. (2014). Assessing the 21st century shift in ENSO variability in terms of the Bjerknes stability index. *Journal of Climate*, 27, 2577–2587. <https://doi.org/10.1175/JCLI-D-13-00438.1>
- Marathe, S., Ashok, K., Swapna, P., & Sabin, T. P. (2015). Revisiting El Niño Modokis. *Climate Dynamics*, 45(11), 3527–3545. <https://doi.org/10.1007/s00382-015-2555-8>
- Marshall, A. G., Hendon, H. H., Feng, M., & Schiller, A. (2015). Initiation and amplification of the Ningaloo Niño. *Climate Dynamics*, 45(9), 2367–2385. <https://doi.org/10.1007/s00382-015-2477-5>
- McPhaden, M. J., Zebiak, S. E., & Glantz, M. H. (2006). ENSO as an integrating concept in earth science. *Science*, 314(5806), 1740–1745. <https://doi.org/10.1126/science.1132588>
- Nagura, M., & McPhaden, M. J. (2021). Interannual variability in sea surface height at southern mid-latitudes of the Indian Ocean. *Journal of Physical Oceanography*, 51(5), 1595–1609. <https://doi.org/10.1175/jpo-d-20-0279.1>
- Rathore, S., Bindoff, N. L., Ummenhofer, C. C., Phillips, H. E., & Feng, M. (2020). Near-surface salinity reveals the oceanic sources of moisture for Australian precipitation through atmospheric moisture transport. *Journal of Climate*, 33(15), 6707–6730. <https://doi.org/10.1175/jcli-d-19-0579.1>
- Rathore, S., Bindoff, N. L., Ummenhofer, C. C., Phillips, H. E., Feng, M., & Mishra, M. (2021). Improving Australian rainfall prediction using sea surface salinity. *Journal of Climate*, 34, 1–56. <https://doi.org/10.1175/jcli-d-20-0625.1>
- Reynolds, R. W., Smith, T. M., Liu, C., Chelton, D. B., Casey, K. S., & Schlax, M. G. (2007). Daily high-resolution-blended analyses for sea surface temperature. *Journal of Climate*, 20, 5473–5496. <https://doi.org/10.1175/2007JCLI1824.1>
- Santoso, A., Mcphaden, M. J., & Cai, W. (2017). The defining characteristics of ENSO extremes and the strong 2015/2016 El Niño. *Reviews of Geophysics*, 55(4), 1079–1129. <https://doi.org/10.1002/2017rg000560>
- Student. (1908). The probable error of a mean. *Biometrika*, 6, 1–25. <https://doi.org/10.2307/2331554>
- Taschetto, A. S., & England, M. H. (2009). El Niño Modoki impacts on Australian rainfall. *Journal of Climate*, 22(11), 3167–3174. <https://doi.org/10.1175/2008jcli2589.1>
- Tozuka, T., Feng, M., Han, W., Kido, S., & Zhang, L. (2021). The Ningaloo Niño/Niña: Mechanisms, relation with other climate modes and impacts. *Tropical and Extratropical Air-Sea Interactions*, 207–219. <https://doi.org/10.1016/b978-0-12-818156-0.00006-x>
- Waliser, D. E., & Graham, N. E. (1993). Convective cloud systems and warm-pool sea surface temperatures: Coupled interactions and self-regulation. *Journal of Geophysical Research*, 98(D7), 12881–12893. <https://doi.org/10.1029/93jd00872>
- Wang, C., & Wang, X. (2013). Classifying El Niño Modoki I and II by different impacts on rainfall in Southern China and typhoon tracks. *Journal of Climate*, 26, 1322–1338. <https://doi.org/10.1175/jcli-d-12-00107.1>
- Wang, M., Du, Y., Qiu, B., Xie, S. P., & Feng, M. (2019). Dynamics on seasonal variability of EKE associated with TIWs in the eastern equatorial Pacific Ocean. *Journal of Physical Oceanography*, 49(6), 1503–1519. <https://doi.org/10.1175/jpo-d-18-0163.1>
- Xie, P., & Arkin, P. A. (1997). Global precipitation: A 17-year monthly analysis based on gauge observations, satellite estimates, and numerical model outputs. *Bulletin of the American Meteorological Society*, 78(11), 2539–2558. [https://doi.org/10.1175/1520-0477\(1997\)078<2539:gpayma>2.0.co;2](https://doi.org/10.1175/1520-0477(1997)078<2539:gpayma>2.0.co;2)
- Yeh, S. W., Kug, J. S., Dewitte, B., Kwon, M. H., Kirtman, B. P., & Jin, F. F. (2009). El Niño in a changing climate. *Nature*, 461(7263), 511–514. <https://doi.org/10.1038/nature08316>
- Zelle, H., Appeldoorn, G., Burgers, G., & van Oldenborgh, G. J. (2004). The relationship between sea surface temperature and thermocline depth in the eastern equatorial Pacific. *Journal of Physical Oceanography*, 34(3), 643–655. <https://doi.org/10.1175/2523.1>
- Zhang, L., & Han, W. (2018). Impact of Ningaloo Niño on tropical Pacific and an interbasin coupling mechanism. *Geophysical Research Letters*, 45(20), 11–300. <https://doi.org/10.1029/2018gl078579>
- Zhao, M., Hendon, H. H., Yin, Y., & Alves, O. (2016). Variations of upper-ocean salinity associated with ENSO from PEODAS reanalyses. *Journal of Climate*, 29(6), 2077–2094. <https://doi.org/10.1175/jcli-d-15-0650.1>
- Zheng, S., Feng, M., Du, Y., Cheng, X., & Li, J. (2016). Annual and interannual variability of the tropical instability vortices in the equatorial eastern Pacific observed from Lagrangian surface drifters. *Journal of Climate*, 29, 9163–9177. <https://doi.org/10.1175/jcli-d-16-0124.1>
- Zinke, J., Hoell, A., Lough, J. M., Feng, M., Kuret, A. J., Clarke, H., et al. (2015). Coral record of southeast Indian Ocean marine heatwaves with intensified Western Pacific temperature gradient. *Nature Communications*, 6(1), 1–9. <https://doi.org/10.1038/ncomms9562>
- Zuo, H., Balmaseda, M. A., Tietsche, S., Mogensen, K., & Mayer, M. (2019). The ECMWF operational ensemble reanalysis–analysis system for ocean and sea ice: A description of the system and assessment. *Ocean Science*, 15, 779–808. <https://doi.org/10.5194/os-15-779-2019>